ACCEPTED VERSION

Siew Yee Lim, Cheryl Suwen Law, Marijana Markovic, Jason K. Kirby, Andrew D. Abell, and Abel Santos

Engineering the slow photon effect in photoactive nanoporous anodic alumina gradient-index filters for photocatalysis

ACS Applied Materials and Interfaces, 2018; 10(28):24124-24136

This document is the Accepted Manuscript version of a Published Work that appeared in final form in ACS Applied Materials and Interfaces, copyright © 2018 American Chemical Society after peer review and technical editing by the publisher. To access the final edited and published work see http://dx.doi.org/10.1021/acsami.8b05946

PERMISSIONS

http://pubs.acs.org/page/4authors/jpa/index.html

The new agreement specifically addresses what authors can do with different versions of their manuscript – e.g. use in theses and collections, teaching and training, conference presentations, sharing with colleagues, and posting on websites and repositories. The terms under which these uses can occur are clearly identified to prevent misunderstandings that could jeopardize final publication of a manuscript **(Section II, Permitted Uses by Authors)**.

Easy Reference User Guide

7. Posting Accepted and Published Works on Websites and Repositories: A digital file of the Accepted Work and/or the Published Work may be made publicly available on websites or repositories (e.g. the Author's personal website, preprint servers, university networks or primary employer's institutional websites, third party institutional or subject-based repositories, and conference websites that feature presentations by the Author(s) based on the Accepted and/or the Published Work) under the following conditions:

• It is mandated by the Author(s)' funding agency, primary employer, or, in the case of Author(s) employed in academia, university administration.
• If the mandated public availability of the Accepted Manuscript is sooner than 12 months after online publication of the Published Work, a waiver from the relevant institutional policy should be sought. If a waiver cannot be obtained, the Author(s) may sponsor the immediate availability of the final Published Work through participation in the ACS AuthorChoice program—for information about this program see http://pubs.acs.org/page/policy/authorchoice/index.html.
• If the mandated public availability of the Accepted Manuscript is not sooner than 12 months after online publication of the Published Work, the Accepted Manuscript may be posted to the mandated website or repository. The following notice should be included at the time of posting, or the posting amended as appropriate:
"This document is the Accepted Manuscript version of a Published Work that appeared in final form in [JournalTitle], copyright © American Chemical Society after peer review and technical editing by the publisher. To access the final edited and published work see [insert ACS Articles on Request author-directed link to Published Work, see http://pubs.acs.org/page/policy/articlesonrequest/index.html]."
• The posting must be for non-commercial purposes and not violate the ACS' "Ethical Guidelines to Publication of Chemical Research" (see http://pubs.acs.org/ethics).
• Regardless of any mandated public availability date of a digital file of the final Published Work, Author(s) may make this file available only via the ACS AuthorChoice Program. For more information, see http://pubs.acs.org/page/policy/authorchoice/index.html.

17 October 2019

http://hdl.handle.net/2440/113821

ACS APPLIED MATERIALS & INTERFACES

Subscriber access provided by UNIVERSITY OF ADELAIDE LIBRARIES

Functional Nanostructured Materials (including low-D carbon)

Engineering the Slow Photon Effect in Photoactive Nanoporous Anodic Alumina Gradient-Index Filters for Photocatalysis

Siew Yee Lim, Cheryl Suwen Law, Marijana Markovic, Jason K. Kirby, Andrew D. Abell, and Abel Santos

ACS Appl. Mater. Interfaces, **Just Accepted Manuscript** • DOI: 10.1021/acsami.8b05946 • Publication Date (Web): 25 Jun 2018

Downloaded from http://pubs.acs.org on June 25, 2018

Just Accepted

"Just Accepted" manuscripts have been peer-reviewed and accepted for publication. They are posted online prior to technical editing, formatting for publication and author proofing. The American Chemical Society provides "Just Accepted" as a service to the research community to expedite the dissemination of scientific material as soon as possible after acceptance. "Just Accepted" manuscripts appear in full in PDF format accompanied by an HTML abstract. "Just Accepted" manuscripts have been fully peer reviewed, but should not be considered the official version of record. They are citable by the Digital Object Identifier (DOI®). "Just Accepted" is an optional service offered to authors. Therefore, the "Just Accepted" Web site may not include all articles that will be published in the journal. After a manuscript is technically edited and formatted, it will be removed from the "Just Accepted" Web site and published as an ASAP article. Note that technical editing may introduce minor changes to the manuscript text and/or graphics which could affect content, and all legal disclaimers and ethical guidelines that apply to the journal pertain. ACS cannot be held responsible for errors or consequences arising from the use of information contained in these "Just Accepted" manuscripts.

ACS Publications

is published by the American Chemical Society. 1155 Sixteenth Street N.W., Washington, DC 20036

Published by American Chemical Society. Copyright © American Chemical Society. However, no copyright claim is made to original U.S. Government works, or works produced by employees of any Commonwealth realm Crown government in the course of their duties.

Engineering the Slow Photon Effect in Photoactive Nanoporous Anodic Alumina Gradient-Index Filters for Photocatalysis

Siew Yee Lim[1,2,3], Cheryl Suwen Law[1,2,3], Marijana Markovic[4,5], Jason K. Kirby[5], Andrew D. Abell[2,3,6], and Abel Santos[1,2,3*]*

[1]School of Chemical Engineering, The University of Adelaide, Engineering North Building, SA 5005 Adelaide, Australia.
[2]Institute for Photonics and Advanced Sensing (IPAS), The University of Adelaide, SA 5005 Adelaide, Australia.
[3]ARC Centre of Excellence for Nanoscale BioPhotonics (CNBP), The University of Adelaide, SA 5005 Adelaide, Australia.
[4]School of Agriculture Food and Wine, The University of Adelaide, SA 5064 Adelaide, Australia.
[5]CSIRO Land and Water, SA 5064 Adelaide, Australia.
[6]Department of Chemistry, The University of Adelaide, SA 5005 Adelaide, Australia.
*E-mails: andrew.abell@adelaide.edu.au ; abel.santos@adelaide.edu.au

KEYWORDS: Nanoporous Anodic Alumina, Photonic Crystals, Slow Photon Effect, Surface Modification, Photocatalysis.

ABSTRACT: In this study, we explore for the first time the capabilities of nanoporous anodic alumina gradient-index filters (NAA-GIFs) functionalized with titanium dioxide (TiO_2) photoactive layers to enhance photon-to-electron conversion rates and improve the efficiency of photocatalytic reactions by 'slow photon' effect. A set of NAA-GIFs was fabricated by sinusoidal pulse anodization, in which a systematic modification of various anodization parameters (i.e. pore widening time, anodization period and anodization time) enables the fine-tuning of the photonic stopband (PSB) of these nanoporous photonic crystals (PCs) across the spectral regions. The surface of NAA-GIFs was chemically modified with photoactive layers of TiO_2 to create a composite photoactive material with precisely engineered optical properties. The photocatalytic performance of TiO_2-functionalized NAA-GIFs was assessed by studying the photodegradation of three model organic dyes (i.e. methyl orange, rhodamine B and methylene blue) with well-defined absorption bands across different spectral regions under simulated irradiation conditions. Our study demonstrates that when the edges of characteristic PSB of TiO_2-modified NAA-GIFs are completely or partially aligned with the absorption band of the organic dyes, the photodegradation rate is enhanced due to 'slow photon' effect. A rational design of the photocatalyst material with respect to the organic dye is demonstrated to be optimal to speed up photocatalytic reactions by an efficient management of photons from high irradiance spectral regions. This provides new opportunities to develop high-performing photocatalytic materials for efficient photocatalysis with broad applicability.

INTRODUCTION

Heterogeneous photocatalysis (henceforth "photocatalysis") is a light-driven process in which photons (light – electromagnetic waves) interact with atoms (matter – semiconductors) to generate electron–hole (e^-/h^+) pairs that can subsequently produce free radicals able to undergo secondary reactions.[1] Among other applications, photocatalysis enables the production of clean hydrogen energy[2], sanitation of water[3], air purification[4], ammonia (NH_3) generation[5], and carbon dioxide (CO_2) reduction[6]. However, most of semiconductor materials have a relatively large energy band gap (~3–5 eV), which constrains their photocatalytic activity to the UV region (only ~5% of the solar spectrum), preventing the efficient utilization of sunlight for practical photocatalytic applications.

Photonic crystals (PCs) are periodic optical micro/nanostructures with forbidden photonic bands that alter the motion of photons when light travels across the PC's structure. The photonic band structure of PCs predicts the propagation of photons with reduced group velocity (v_g) at those directions close to the blue and red edges of the PCs' photonic stopband (PSB), where the band becomes almost flat ('slow photons' with $v_g \sim 0$).[7] In semiconductor PCs, light absorption enhancement by slow photon effect is precisely engineered by the PCs' structure to generate extra e^-/h^+ pairs at those spectral regions where the semiconductor absorbs light poorly (e.g. TiO_2 in the visible/infrared) to enhance photon-to-electron conversion rates.[8-11] Nanoporous semiconductor PCs are of particular importance since these nanostructures offer: i) light-trapping capabilities to collect photons at high-irradiance spectral regions (e.g. visible), ii) efficient percolation pathways for vectoral transfer of photo-promoted electrons, iii) high specific surface area that increases the number of photo-active centers for redox reactions, and iv) nanoporous structure that facilitates mass transport of molecular species involved in redox reactions. Some proof-of-concept studies have identified

'slow photon' effects in inverted opal PCs. However, these nanostructures have limited versatility to tune the features of the PSB, are restricted to 3D nanostructures, feature defects that act as light scattering centers, require long synthesis processes, and are constrained to small areas.[12]

Some studies to date have demonstrated the fabrication of nanotubular TiO_2-based PCs by electrochemical oxidation (i.e. anodization) of titanium substrates.[13,14] However, anodization of titanium does not allow sufficient control of the nanotubular structure of TiO_2 to create PC structures with versatile PSB since the hydrofluoric acid (HF)-based electrolytes used progressively etch the nanotubes' walls during the anodization process.[15] Alternative nanoporous materials, such as nanoporous anodic alumina (NAA), can address these limitations. NAA produced by anodization of aluminum in fact provides an excellent platform to develop PC structures due to its highly controllable and flexible nanoporous geometry, which can be precisely modulated in depth to engineer its effective medium and create multi-dimensional (1D, 2D and 3D) NAA-PCs with versatile PSB across the spectral regions.[16-23] NAA-PCs such as gradient-index filters[16], optical microcavities[22] and distributed Bragg reflectors[23] present as ideal platforms to utilize the 'slow photon' effect for enhanced photocatalytic reactions. However, the wide energy bandgap of NAA (i.e. 7.0–9.5 eV, deep UV region)[24,25] prevents the direct use of NAA-PCs for photocatalysis. Despite this intrinsic limitation, the chemical modification of NAA-PCs with photoactive materials such as TiO_2 does provide an opportunity to develop new platform materials as highly efficient photocatalysts by a rational management of photons at the nanoscale.

Herein, we present the first rationally designed photocatalyst material based on a TiO_2-functionalized nanoporous anodic alumina gradient-index filter (NAA-GIF) as a platform to achieve enhanced photocatalytic performances. NAA-GIFs are synthesized by sinusoidal pulse anodization (SPA) approach and subsequently functionalized with

photoactive layers of TiO_2 through sol-gel method (**Figure 1a**). We perform a systematic study on the effect of the PSB's features of photoactive NAA-GIFs, controlled by the anodization parameters (i.e. anodization period, anodization time and pore widening time), on the photocatalytic performance of these PC structures (**Figures 1b and c**). Photocatalytic degradation of three model organic dyes (i.e. methyl orange–MO, methylene blue–MB and rhodamine B–RhoB) in these photoactive NAA-PCs provides a reference to identify and quantify slow photon effects for enhanced photocatalytic performances.

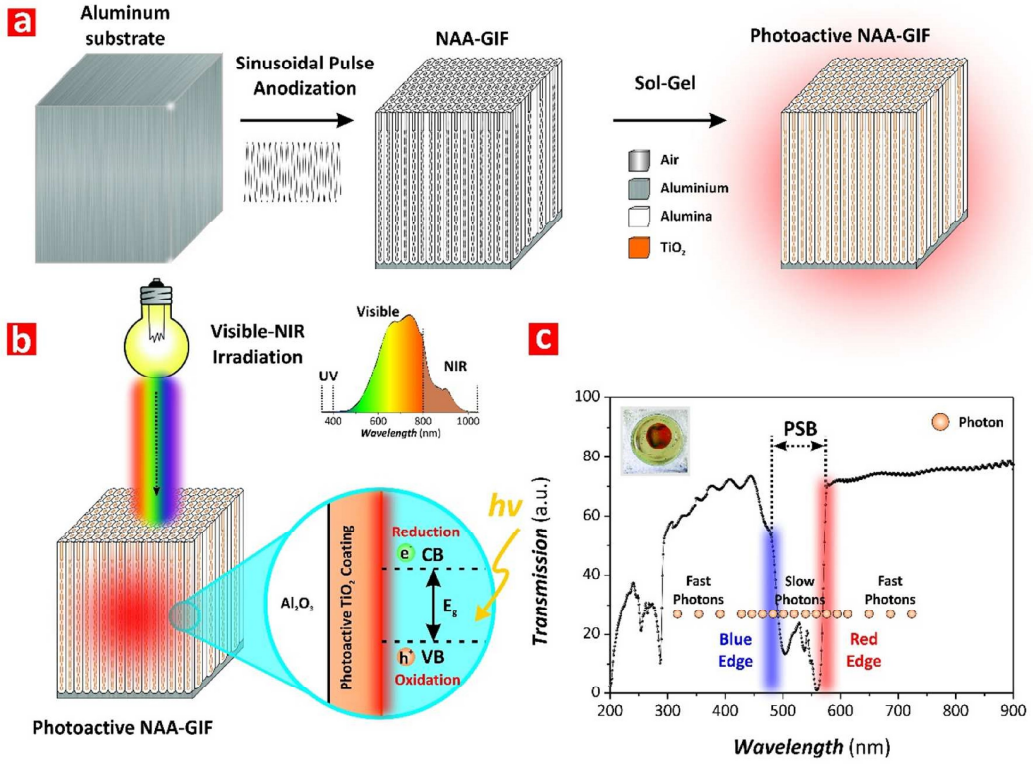

Figure 1. Conceptual illustration of the development and applicability of photoactive NAA-GIFs for photocatalysis. a) Schematic representing the fabrication process of photoactive NAA-GIFs by sinusoidal pulse anodization (SPA) (left) and deposition of photoactive TiO_2 layers by sol-gel method (right). b) Schematic showing the utilization of TiO_2-functionalized NAA-GIFs in photocatalysis under controlled visible-NIR irradiation conditions with details showing the chemical and electronic band structures of these composite photocatalysts, where CB = conduction band, VB = valence band, E_g = band gap energy level, and $h\nu$ = excitation energy. c) Transmission spectrum of a TiO_2-functionalized NAA-GIF showing the blue and red edges of the photonic stopband (PSB) where photons slow down their group velocity after interacting with the PC structure (inset: digital image of that NAA-GIF structure produced with T_P = 650 s, A_J = 0.420 mA cm^{-2}, J_{Offset} = 0.280 mA cm^{-2}, t_{An} = 20 h and t_{pw} = 6 min).

EXPERIMENTAL SECTION

2.1. Materials. High purity (99.9997 %) aluminum (Al) foils 0.32 mm thick were purchased from Goodfellow Cambridge Ltd. (UK) and used to produce NAA-GIFs by SPA. Sulfuric acid (H_2SO_4), phosphoric acid (H_3PO_4), hydrochloric acid (HCl), copper (II) chloride ($CuCl_2$), ethanol (EtOH – C_2H_5OH), titanium (IV) butoxide ($Ti(OBu)_4$), hydrogen peroxide (H_2O_2), methyl orange (MO), methylene blue (MB) and rhodamine B (RhoB) were supplied by Sigma-Aldrich (Australia) and used as received, without additional purification steps. Ultrapure Mili-Q® water (18.2 MΩ cm) was used for the preparation of all the aqueous solutions in this study.

2.2. Fabrication of NAA-GIFs. NAA-GIFs were produced by sinusoidal pulse anodization (SPA) approach under current density control conditions.[16] 1.5 x 1.5 cm^2 Al square chips were cleaned in EtOH and water under sonication for 15 min each and dried under air stream to remove any organic residues. These Al substrates were subsequently electropolished in a mixture of EtOH and $HClO_4$ 4:1 (*v*:*v*) at 20 V and 5 ^oC for 3 min. After electropolishing, the Al substrates were anodized at -1 ^oC in a 1.1 M H_2SO_4 aqueous solution with 25 *v*% of EtOH to prevent it from freezing at temperatures below 0 ^oC.[26,27] The anodization process started with a constant current density of 1.120 mA cm^{-2} for 1 h to achieve a homogeneous pore growth prior to SPA. The anodization profile was subsequently switched to sinusoidal pulse mode, where the anodization current density was pulsed between high (J_{Max} = 1.120 mA cm^{-2}) and low (J_{Min} = 0.280 mA cm^{-2}) current density values following **Equation 1**:

$$J(t) = A_J \left[\sin\left(\frac{2\pi}{T_P}t\right) + 1\right] + J_{Offset} \quad (1)$$

where $J(t)$ is the current density at a given time t, A_J is the current density amplitude, T_P is the anodization period and J_{Offset} is the current density offset.

NAA-GIFs provide an excellent platform to study 'slow photon' effects due to their versatile PSB, the features of which (i.e. position of central wavelength and bandwidth) can be precisely engineered across the spectral regions by SPA. To investigate the effect of the anodization period (T_P) and the anodization time (t_{An}) on the photocatalytic performance of TiO_2-modified NAA-GIFs, we fabricated a set of NAA-GIFs with fixed A_J and J_{Offset} at 0.420 mA cm^{-2} and 0.280 mA cm^{-2}, respectively. In the first set of NAA-GIFs, T_P was systematically modified from 550 to 850 s, with ΔT_P = 100 s at fixed t_{An} = 20 h. The second set of NAA-GIFs was fabricated with varying t_{An} from 5 to 20 h, with Δt_{An} = 5 h and fixed T_P = 850 s. Note that NAA-GIFs were pore widened in an aqueous solution of 5 *wt*% H_3PO_4 at 35 ^oC. The pore widening time (t_{pw}) was modified from 0 to 6 min with Δt_{pw} = 2 min.

2.3. Surface Functionalization of NAA-GIFs with TiO_2. The surface of NAA-GIFs produced with different T_P (i.e. 550, 650, 750 and 850 s) and t_{An} (i.e. 5, 10, 15 and 20 h) at t_{pw} = 6 min was chemically functionalized with photoactive layers of TiO_2 through sol-gel method.[28] TiO_2 sol was prepared in a beaker by magnetically mixing a mixture of titanium (IV) butoxide (3 mol%) and EtOH (97 mol%) for 10 min. NAA-GIFs were then dip-coated in the TiO_2 sol for 24 h. The surface-modified NAA-GIFs were subsequently washed with EtOH to remove any excess TiO_2 sol and titanium (IV) butoxide from the inner surface of these nanoporous PCs. After washing, the composite TiO_2-NAA-GIFs were dried in an oven at 50 ^oC for 10 min to evaporate any residual EtOH.

2.4. Optical Characterization. Prior to optical characterization, NAA-GIFs were chemically etched in a saturated solution of $HCl/CuCl_2$ using a 5 mm diameter circular window etching mask to dissolve the remaining Al substrate from the backside. Transmission spectra of

chemically etched and pore widened NAA-GIFs, fabricated with different anodization parameters, were obtained in air and water from 200 to 800 nm at normal incidence (i.e. $\theta = 0^o$) using a UV-visible spectrophotometer (Cary 300, Agilent, USA). The absorption spectra of 5 mg L^{-1} organic dyes solution in a polystyrene cuvette of 10 mm path length were acquired from 200 to 800 nm to determine the absorption band of organic dyes (i.e. MO, MB and RhoB). To characterize the interferometric color of NAA-GIFs, digital pictures with a black background were acquired using a Canon EOS 700D digital camera, which was equipped with a Tamron 90 mm F2.8 VC USD macro mount lens with autofocus function under natural light illumination.

2.5. Photocatalytic Degradation of Organic Dyes. The photocatalytic performance of TiO_2-modified NAA-GIFs produced with different T_P and t_{An} was assessed by monitoring the photocatalytic degradation of three different organic dyes with well-defined absorption bands (i.e. MO – $\lambda_{Abs\text{-}MO}$ = 464 nm, RhoB – $\lambda_{Abs\text{-}RhoB}$ = 554 nm and MB – $\lambda_{Abs\text{-}MB}$ = 664 nm) under simulated solar light irradiation conditions. 2 mL of a mixture of 5 mg L^{-1} of dye and 0.1 M H_2O_2 solution was pipetted into a transparent cuvette. The TiO_2-functionalized NAA-GIFs, which had an effective area of 1 cm^2, were then placed in the cuvette filled with the dye mixture. The solutions was magnetically stirred in a dark vessel (solar simulator) for 30 min to achieve the adsorption-desorption equilibrium prior to irradiation. This was then illuminated with simulated solar light irradiation using a 150 W (~3000 lumen) halogen lamp (HL250-A, Amscope, Australia) at room temperature. To determine the concentration of dye at specific time intervals, the absorbance of the absorption band of the solution at each illumination time interval (i.e. 30 min) was analyzed by a UV-visible spectrophotometer. Calibration lines establishing the relationship between the solution absorbance and the concentration of each dye were used to determine the photocatalytic conversion ratio (C_t/C_o), where C_o is the concentration of solution after stirring in the dark for 30 min and C_t is the

concentration at illumination time t (**Figure S1 – Supporting Information**). This parameter was evaluated to determine the kinetic model for this photocatalytic system as a function of the TiO_2-NAA-GIFs and the model dye molecule. Note that these experiments were also performed with non-functionalized NAA-GIFs (i.e. NAA-GIFs without TiO_2 functional layer), which were used as control samples.

2.6. Chemical and Structural Characterization. The morphology and geometric features of NAA-GIFs were characterized using a field emission gun scanning electron microscopy (FEG-SEM FEI Quanta 450). FEG-SEM images acquired were analyzed by ImageJ (public domain program developed at the RSB of the NIH).[29] The chemical composition of NAA-GIFs before and after surface functionalization with TiO_2 were analyzed by energy dispersive X-ray (EDX) spectroscopy during FEG-SEM characterization. The chemical structure of NAA-GIFs was further characterized by Fourier transform infrared (FTIR Nicolet 6700) spectroscopy and X-ray diffraction (XRD Rigaku MiniFlex 600).

RESULTS AND DISCUSSION

3.1. Structural Characterization of NAA-GIFs. Figure 2 presents a set of representative FEM-SEM images of the NAA-GIFs produced in this study. A top view FEG-SEM image is shown in **Figure 2a** to reveal evenly and randomly distributed nanopores of NAA-GIFs across the surface, where the average pore diameter (d_P) was measured to be 17 ± 3 nm after a pore widening treatment of 6 min. The cross-sectional view FEG-SEM images (**Figure 2b and c**) show the in-depth modulation of porosity of NAA-GIFs following the sinusoidal current density profile applied during SPA. The distance between adjacent layers with sinusoidally modulated porosity, defined as the period length (L_{TP}), correspond to each pulse in the SPA profile and it is visually indicated by the white arrowheads shown in **Figure 2c**. The image analysis revealed a linear correlation between the anodization period (T_P) and L_{TP}, where L_{TP} increases at a rate of 0.34 nm s^{-1} with increasing T_P (**Figure 2d**).

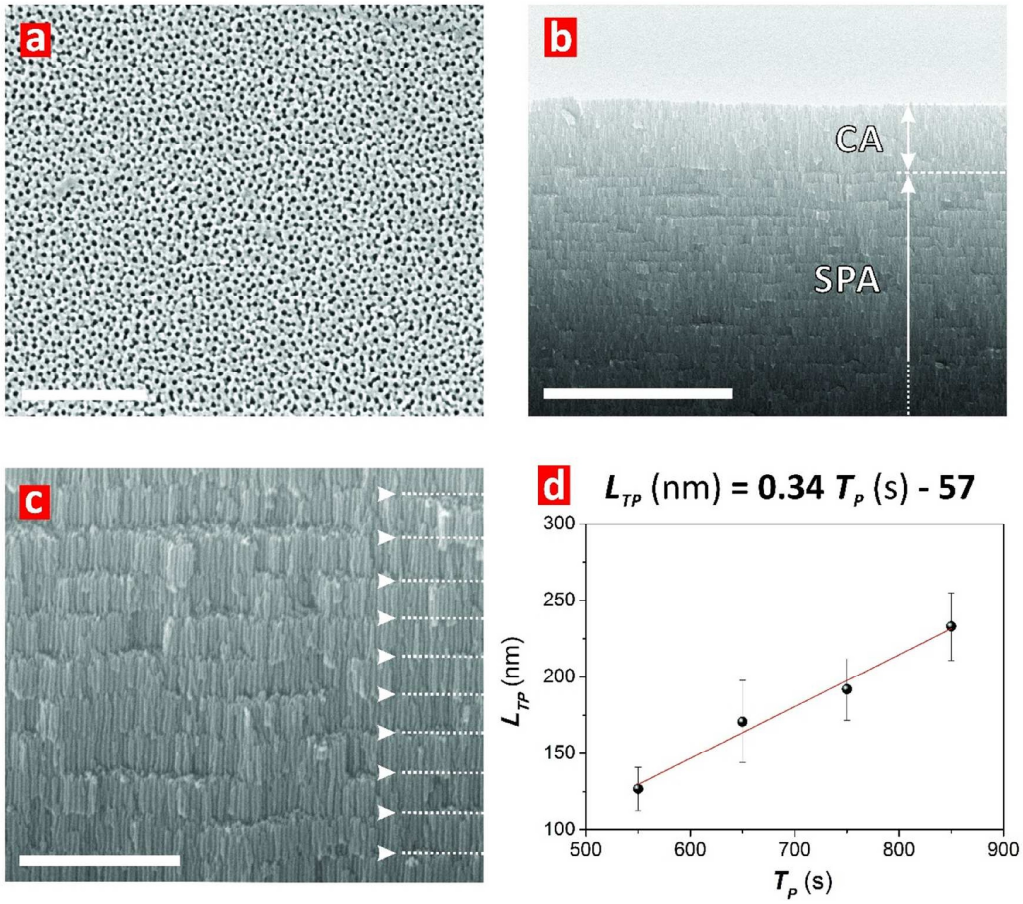

Figure 2. Representative FEG-SEM images of NAA-GIFs produced by the sinusoidal pulse anodization (SPA). a) Top view FEG-SEM image of a NAA-GIF produced with T_P = 850 s, A_J = 0.420 mA cm^{-2}, J_{Offset} = 0.280 mA cm^{-2}, t_{An} = 20 h and t_{pw} = 6 min (scale bar = 500 nm). b) General cross-sectional view FEG-SEM image of a NAA-GIF, where CA and SPA represent the constant (CA) and sinusoidal pulse (SPA) modes, respectively (scale bar = 5 µm). c) Magnified view of (b) showing details of the nanoporous structure of NAA-GIFs (scale bar = 1 µm) (Note: the layer between each consecutive white arrowheads denote the period length – L_{TP}). d) Linear relationship between the period length (L_{TP}) and anodization period (T_P) in NAA-GIFs.

3.2. Effect of the Anodization Parameters on the Optical Properties of NAA-GIFs. **Figure S2 (Supporting Information)** shows the intrinsic relationship between the fabrication parameters (i.e. anodization period (T_P), pore widening time (t_{pw}), and anodization time (t_{An}) or number of anodization pulses (N_P = t_{An}/T_P)) with the optical properties (i.e. central wavelength (λ_C) of the PSB and interferometric color) of NAA-GIFs. The combined effect of T_P and t_{pw} on the position of the characteristic PSB of NAA-GIFs was systematically studied by modifying T_P from 550 to 850 s with ΔT_P = 100 s, and t_{pw} from 0 to 6 min with Δt_{pw} = 2 min, at a fixed t_{An} of 20 h (**Figure S2a**). Linear fittings demonstrate the correlation

between T_P and λ_C, of which the slopes of the linear fittings were found to be 0.79 ± 0.09, 0.81 ± 0.12, 0.65 ± 0.16 and 0.78 ± 0.16 nm s^{-1} for t_{pw} = 0, 2, 4 and 6 min, respectively. The position of the PSB of these NAA-GIFs can be tuned from 415 ± 1 nm (T_P = 550 s and t_{pw} = 6 min) to 715 ± 1 nm (T_P = 850 s and t_{pw} = 0 min) within the range of fabrication parameters studied. This analysis demonstrates that λ_C red-shifts with T_P, where the optical characteristic of NAA-GIFs shows the strongest dependence on T_P at t_{pw} = 2 min (i.e. sharpest slope – 0.81 ± 0.12 nm s^{-1}). As per previous studies,[16] λ_C blue-shifts its position with t_{pw}. **Figure S2b** illustrates the combined effect of t_{An} (or N_P) and t_{pw} on the λ_C of NAA-GIFs, where t_{An} was systematically modified from 5 to 20 h (i.e. from 22 to 85 pulses) with an interval of 5 h (i.e. 21 pulses), and t_{pw} from 0 to 6 min with an interval of 2 min, while T_P was fixed at 850 s. This graph denotes that λ_C fluctuates around an average value with t_{An} (N_P) and blue-shifts its position with t_{pw}.[16] **Figures S2c and d** compile digital pictures of NAA-GIFs produced with different T_P and t_{An} as a function of t_{pw}, respectively. The digital images shown in **Figure S2c** reveal that as produced NAA-GIFs (i.e. t_{pw} = 0 min) display vivid colors such as blue and red-orange for T_P = 550 and 650 s, respectively. However, these NAA-GIFs are transparent (i.e. black background – NIR region) for T_P = 750 and 850 s at t_{pw} = 0 min. Note that the interferometric color correlates with the position of the characteristic PSB within the UV-visible-NIR spectrum. As t_{pw} increases, the interferometric color of NAA-GIFs is blue-shifted, becoming blue, cyan, chartreuse and yellow at t_{pw} = 6 min for NAA-GIFs produced at T_P = 550, 650, 750 and 850 s, respectively. This effect is also observed for NAA-GIFs produced at different anodization times. **Figure S2d** shows digital pictures of NAA-GIFs produced at t_{An} = 5, 10, 15 and 20 h. At t_{pw} = 0 min, all the NAA-GIFs have located their PSB in the NIR range of the spectrum (i.e. transparent). As t_{pw} increases, the PSB is blue-shifted to the visible range and interferometric colors rise. NAA-GIFs produced at t_{An} = 5, 10, 15 and 20 h display vivid green, orange, chartreuse and yellow color at t_{pw} = 6 min. To summarize,

the anodization parameters T_P, t_{An} and t_{pw} can be used to engineer the optical properties (i.e. λ_C and interferometric color) of NAA-GIFs. All the anodization parameters allow the precise tuning of the position of characteristic PSB of NAA-GIFs across the entire UV-visible-NIR spectrum.

3.3. Chemical Analysis of TiO_2-Functionalized NAA-GIFs. Photoactive NAA-GIFs were produced by modifying the inner surface of NAA-GIFs with photoactive layers of TiO_2 deposited by sol-gel method. **Figure S3 (Supporting Information)** shows energy dispersive X-ray (EDX), Fourier Transform Infrared (FTIR) and X-ray diffraction (XRD) spectra of NAA-GIFs before and after surface functionalization. These analyses demonstrate successful TiO_2-modification of the inner surface of NAA-GIFs after 24 h. **Figure S3a** shows the EDX spectrum of as-produced NAA-GIFs, which shows the characteristic peaks of O (12%), Al (79%), P (4%) and S (5%). These elements correspond to the alumina structure (Al_2O_3) contaminated by sulfur and phosphorus atoms incorporated into the Al_2O_3 structure during the anodization and pore widening steps, respectively. EDX spectrum of TiO_2-functionalized NAA-GIFs shows characteristic peaks of Ti and an increment of the percentage of O atoms, which denote the presence of TiO_2 in the composite structure. The relative percentage of elements in TiO_2-modified NAA-GIFs was found to be O (23%), Al (64%), P (4%), S (5%) and Ti (4%). The confirmation of the successful deposition of TiO_2 onto the inner surfaces of NAA-GIFs is also demonstrated in FTIR analysis (**Figure S3b)**, which shows three main transmission peaks related to TiO_2 after surface functionalization (i.e. 1530, 1622 and 3263 nm). These transmission peaks are in good agreement with those reported in previous studies for TiO_2 nanoparticles.[30,31] XRD spectra of as-produced and TiO2-functionalized NAA-GIFs are shown in **Figure S3c**. As-produced NAA-GIF present three characteristic peaks in their XRD spectra located at 45, 65 and 78^0, which correspond to an amorphous alumina (Al_2O_3) phase. The deposition of the TiO_2 functional layer does not generate any additional peak in

the XRD spectra, indicating that the TiO_2 layer is crystallographically amorphous. However, the position of these peaks undergoes a slight shift in position and decrease their intensity. Thus, our chemical analysis confirms the successful deposition of photoactive layers of TiO_2 onto the inner surface of NAA-GIFs to endow these PC structures with photocatalytic activity.

3.4. Effect of TiO_2 Modification on the Optical Properties of NAA-GIFs. The characteristics of the PSB of photoactive PC structures enable the design and engineering of materials that can make an optimal utilization of the 'slow photon' effect for photocatalysis. The effect of surface functionalization on the optical properties of TiO_2-modified NAA-GIFs was studied by varying the deposition time (t_D) of TiO_2 layers from 0 to 24 h and characterized the position of the PSB (λ_C) and its full-width at half maximum (FWHM) in different media (i.e. air and water) filling the nanoporous network of NAA-GIFs. **Figure 3** shows the effect of TiO_2 surface functionalization of NAA-GIFs produced with different T_P (i.e. 550, 650, 750 and 850 s) and t_{An} (5, 10, 15 and 20 h) at t_{pw} = 6 min and t_D = 0 and 24 h on the features of the PSB of NAA-GIFs. **Figures 3a and b** summarize the dependency of λ_C on t_D and the medium filling the nanopores for the NAA-GIFs assessed in our study. These bar charts demonstrate that, after functionalization with TiO_2 for 24 h, the position of characteristic PSB of NAA-GIFs in air is red-shifted at a rate of 8.9 ± 3.5 nm s^{-1} and 10.5 ± 0.9 nm h^{-1} for T_P and t_{An}, respectively. Modification of the inner surface of NAA-GIFs, with a thin layer of TiO_2, red-shifts progressively the PSB due to the higher refractive index of TiO_2 with respect to Al_2O_3 (i.e. n_{Al2O3} = 1.70 RIU and n_{TiO2} = 2.40 RIU) and the physical reduction of the nanopore diameter of NAA-GIFs. **Figure S4 (Supporting Information)** shows the effect of the deposition time of TiO_2 on the PSB of NAA-GIFs. This slight red shift denotes that the deposited photoactive layer of TiO_2 is thin. In contrast, λ_C undergoes a more significant red-shift when the nanoporous network of surface-modified NAA-GIFs is filled

with water (i.e. media in which the photocatalytic reactions occur). Infiltration of these nanoporous PCs with a medium of a higher refractive index than that of air (i.e. n_{Air} = 1.00 RIU and n_{Water} = 1.33 RIU) leads to a red shift in the position of the characteristic PSB, 69.2 ± 14.7 nm s^{-1} and 80.5 ± 7.6 nm h^{-1} for T_P and t_{An}, respectively. **Figures 3c and d** show the effect of the TiO_2 functionalization and the water infiltration on the FWHM of the PSB of NAA-GIFs produced with various T_P and t_{An}. It is apparent from these figures that FWHM is narrowed at a rate of 29.8 ± 10.3 nm s^{-1} and 12.1 ± 15.8 nm h^{-1} for T_P and t_{An}, respectively, after modifying the inner surface of NAA-GIFs with photoactive TiO_2 layers. Infiltration of the nanopores of TiO_2-functionalized NAA-GIFs with water produces a more significant narrowing of the FWHM. Thus FWHM narrows its width after infiltration at 65.1 ± 28.2 nm s^{-1} and 44.4 ± 23.9 nm h^{-1} for T_P and t_{An}, respectively. The narrowing of the FWHM of the PSB is associated with the light absorption[16,32] by the deposited layer of TiO_2 and the medium filling the nanopores of NAA-GIFs. A comparative analysis of the effect of both factors reveals that the latter (i.e. water infiltration) produces a more significant effect in the narrowing of the FWHM due to the absorption of incoming light by the water molecules. **Figures 3e and f** show representative transmission spectra and schematic illustrations of a NAA-GIF produced with T_P = 750 s and t_{pw} = 6 min at t_D = 0 and 24 h in air and water. This reveals that the position of the characteristic PSB red-shifts while the bandwidth of the PSB is narrowed after surface functionalization with TiO_2 layers and water infiltration. With reference to air, the 2nd order PSB of the NAA-GIF is located at 288 ± 1 nm before surface modification with TiO_2 layers. However, the 2nd order PSB vanishes after the NAA-GIF is modified with TiO_2 layers, which can be associated with the strong light absorption by the TiO_2 layer in the UV region (< 380 nm).[33] This further confirms successful modification of the inner surface of NAA-GIFs with photoactive TiO_2 layers, which is in good agreement

with the results obtained by EDX and FTIR analyses (**Figure S3 – Supporting Information**).

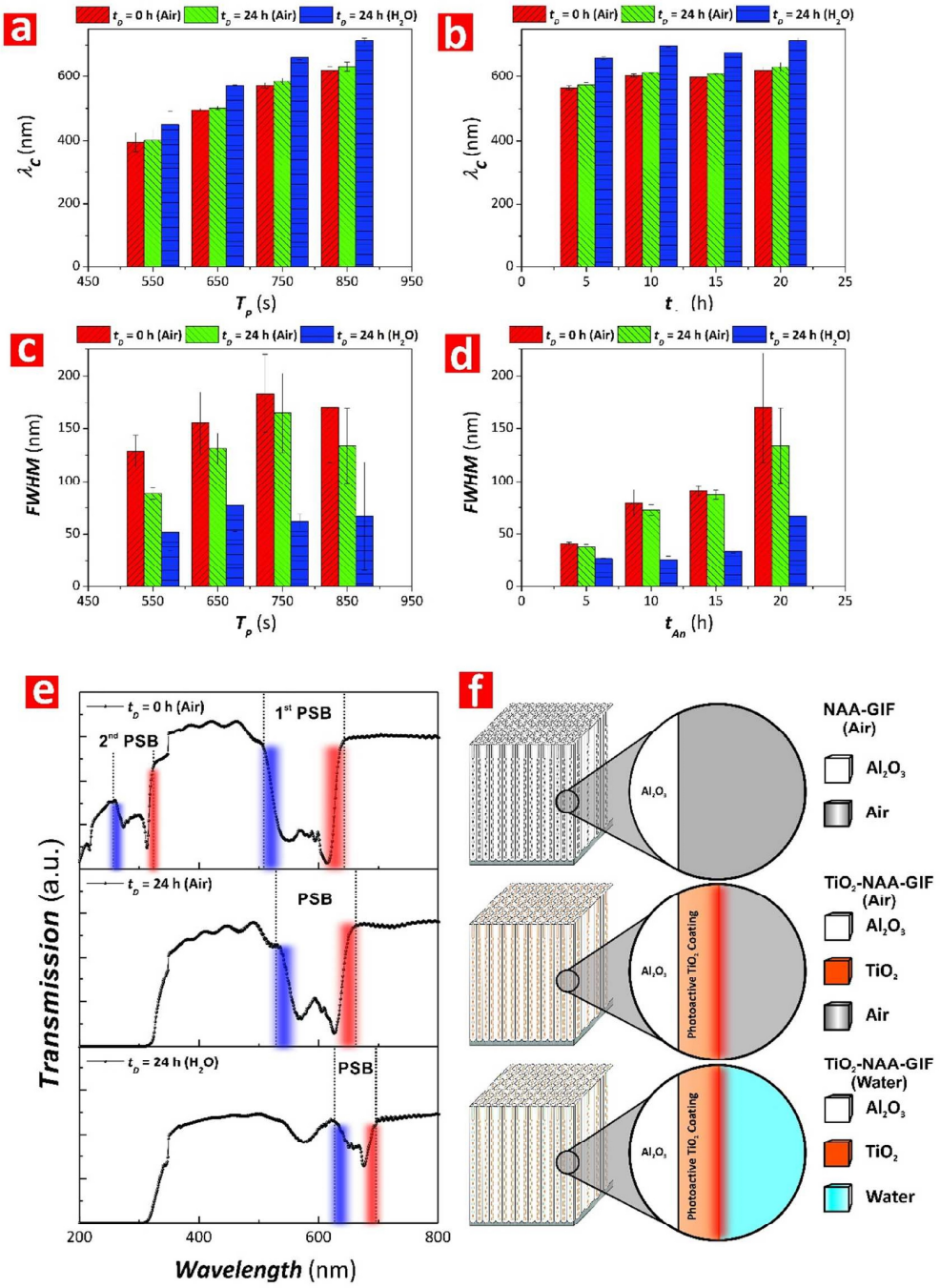

Figure 3. Assessment of optical properties of NAA-GIFs in different media after surface functionalization with TiO_2 layers. a-b) Bar charts showing the effect of surface modification parameters on the position of the central wavelength (λ_C) of NAA-GIFs fabricated with t_{pw} = 6 min and varying T_P (i.e. 550, 650, 750 and 850 s) and t_{An} (i.e. 5, 10, 15 and 20 h), respectively. c-d) Bar charts showing the effect of surface functionalization on the full width at half maximum (FWHM) of NAA-GIFs fabricated with t_{pw} = 6 min and varying T_P (i.e. 550, 650, 750 and 850 s) and t_{An} (i.e. 5, 10, 15 and 20 h), respectively. (e) Representative transmission spectra of a NAA-GIF produced with T_P = 750 s, A_J = 0.420 mA cm^{-2}, J_{Offset} = 0.280 mA cm^{-2}, t_{An} = 20 h and t_{pw} = 6 min showing the evolution of the PSB with the deposition time and the media filling the nanopores (from top to bottom: NAA-GIF in air, TiO_2-functionalized NAA-GIF in air and TiO_2-functionalized NAA-GIF in water. f) Schematic illustration showing the chemical composition and the media filling the nanopores in the scenarios shown in (e).

To summarize, the position and bandwidth of the PSB of NAA-GIFs is precisely tuned across the spectral regions by the manipulation of T_P, t_{An} and t_D. The relationship between fabrication parameters and features of the PSB of photoactive NAA-GIFs provides an optimal platform to study and engineer the 'slow photon' effect for photocatalytic applications. TiO_2 functional layers cannot use photons from the visible and NIR spectral regions for photocatalysis due to its electronic band gap. However, TiO_2-functionalized NAA-GIFs with PSB positioned at the visible and NIR regions can enable the utilization of these high-irradiance sunlight regions to speed up photocatalytic reactions.

3.5. Understanding the 'Slow Photon' Effect in TiO_2-functionalized NAA-GIFs. The photocatalytic performances of TiO_2-modified NAA-GIFs fabricated at t_{pw} = 6 min and different T_P (i.e. 550, 650, 750 and 850 s) and t_{An} (i.e. 5, 10, 15 and 20 h) were assessed by studying the photocatalytic degradation of three model organic dyes (i.e. MO, RhoB and MB) under simulated solar light irradiation. **Figure S5 (Supporting Information)** presents absorption spectra of MO, RhoB and MB with the corresponding absorption bands at 464 nm, 554 nm and 664 nm, respectively. **Figure S6 (Supporting Information)** displays the spectral properties of the artificial illumination used in our study to simulate sunlight irradiation. This graph reveals the spectral distribution to be 0.12% for UV (350–400 nm), 82.60% for visible (400–800 nm) and 17.28% for NIR (800–1025 nm), which is essentially within the visible region. Therefore, liquid-phase photocatalytic degradation of the model organic dyes in our study is mostly driven by visible light irradiation. Note that these reactions were performed with the addition of 0.1 M H_2O_2 solution to aid in the photogeneration of charge carriers in the TiO_2 photoactive layers. The photocatalytic performance of TiO_2-modified NAA-GIFs were measured and fitted to the pseudo-first order kinetics model shown in **Equation 2**:

$$-\ln\left(\frac{C_t}{C_o}\right) = kt \quad (2)$$

where C_o is the adsorption-desorption equilibrium concentration of model dye, C_t is the reaction concentration of model dye at time t and k is the kinetic constant.

The residual concentration of each dye after 2 h of photocatalytic reaction (C_R) where estimated using the calibration lines shown in **Figure S1** and the obtained results are summarized in **Tables S1 and S2 (Supporting Information)**.

3.5.1. Effect of Anodization Period on the Photocatalytic Performance of TiO_2-NAA-GIFs

The origin of the 'slow photon' effect in photoactive NAA-GIFs is associated with the features of the PC's PSB, where photons from the incoming light reduce group velocity at the wavelengths of the blue and red edges of the PSB. As demonstrated, NAA-GIFs are a perfect platform to study this light–matter interaction since the PSB can be engineer with precision and versatility across the spectral regions by SPA. This provides a unique opportunity to control the interaction between photons and the nanoporous PC structure to generate extra e^-/h^+ at those spectral regions where the photocatalyst material is intrinsically limited (i.e. visible and NIR for TiO_2). **Figure 4** and **Table 1** summarize the photocatalytic degradation performances of MO, RhoB and MB in TiO_2-functionalized NAA-GIFs with varying T_P, from 550 to 850 s under controlled illumination conditions. **Figures 4a-c** show the linearized pseudo-first order kinetics for these photocatalytic processes and **Figures 4d-f** show the relationship between the blue and red edges of the characteristic PSB of TiO_2-modified NAA-GIFs and the absorption band of MO, RhoB and MB.

The kinetic constant (k) for the photocatalytic degradation of MO by TiO_2-functionalized NAA-GIFs with T_P = 550, 650, 750 and 850 s were 0.24 ± 0.01, 0.25 ± 0.01, 0.17 ± 0.01 and 0.19 ± 0.01 h^{-1}, respectively (**Figure 4a and Table 1**). k values were higher for TiO_2-modified NAA-GIFs produced with shorter T_P (i.e. 550 and 650 s) than for those fabricated with longer T_P (i.e. 750 and 850 s), indicating that NAA-GIFs produced with shorter

anodization period can photodegrade MO at faster rates than their counterparts produced with longer T_P. For instance, the photodegradation of MO in TiO_2-modified NAA-GIFs fabricated with T_P = 550 s is 29% and 21% faster than that in TiO_2-functionalized NAA-GIFs produced with T_P = 750 and 850 s, respectively. In the case of TiO_2-modified NAA-GIFs fabricated with T_P = 650 s, the photodegradation efficiency difference increases to 32% and 24% as compared to their counterparts fabricated with T_P = 750 and 850 s, respectively.

Table 1. Values of the kinetic constant (k) for the photodegradation of MO, RhoB and MB molecules in TiO_2-functionalized NAA-GIFs produced with T_P = 550, 650, 750 and 850 s.

	Anodization Period			
Organic Dye	550 s	650 s	750 s	850 s
MO	$0.24 \pm 0.01\ h^{-1}$	$0.25 \pm 0.01\ h^{-1}$	$0.17 \pm 0.01\ h^{-1}$	$0.19 \pm 0.01\ h^{-1}$
RhoB	$0.39 \pm 0.02\ h^{-1}$	$0.27 \pm 0.01\ h^{-1}$	$0.30 \pm 0.01\ h^{-1}$	$0.31 \pm 0.01\ h^{-1}$
MB	$1.07 \pm 0.04\ h^{-1}$	$1.84 \pm 0.09\ h^{-1}$	$0.36 \pm 0.01\ h^{-1}$	$2.10 \pm 0.07\ h^{-1}$

This enhancement in photodegradation performance is associated with the 'slow photon' effect in these PC structures. **Figure 4d** reveals that the PSB of TiO_2-modified NAA-GIFs produced with T_P = 550 and 650 s overlaps completely and partially with the absorption band of MO, respectively. The blue (i.e. blue vertical line) and red (i.e. red vertical line) edges of the PSB of TiO_2-functionalized NAA-GIFs with T_P = 550 and 650 s are located within the absorption band of MO (i.e. $\lambda_{Blue\text{-}550s}$ = 466 nm, $\lambda_{Red\text{-}550s}$ = 527 nm, $\lambda_{Blue\text{-}650s}$ = 543 nm, $\lambda_{Red\text{-}650s}$ = 613 nm and $\lambda_{Abs\text{-}MO}$ = 464 nm). Under illumination, groups of incoming photons propagate with strongly reduced group velocity at the vicinity of the PC's PSB and localize in high (i.e. photocatalysts) and low (i.e. dye and pores) dielectric parts of the red and blue edge of the PC's PSB, respectively.[34] Photocatalytic degradation of MO would thus be expected to

be significantly enhanced in those spectral regions where the edges of the PSB are located in the proximity of the absorption band of MO due to enhancement in the photon-to-electron conversion rate.[34-36] Our results and analysis confirm this hypothesis since the PSB of TiO_2-modified NAA-GIFs produced with T_P = 550 and 650 s are within the absorption band of MO. The slightly higher performance shown by TiO_2-NAA-GIFs produced with T_P = 650 s could be associated with the wider PSB of these PC structures (**Figure 3c** – $FWHM_{550s}$ = 52 ± 18 nm and $FWHM_{650s}$ = 77 ± 25 nm) and its relative position with respect to the absorption band of MO (i.e. $\lambda_{C\text{-}550s}$ = 450 ± 4 nm, $\lambda_{C\text{-}650s}$ = 571 ± 2 nm and $\lambda_{Abs\text{-}MO}$ = 464 nm). In contrast, the characteristic PSB of TiO_2-modified NAA-GIFs produced with T_P = 750 and 850 s is located completely outside the absorption band of MO, as shown in **Figure 4d**, where the latter is located the furthest away. In this region, the photocatalytic performance of these photoactive PC structures is independent of the 'slow photon' effect, relying exclusively on the geometric features of the nanoporous PC structure and the irradiation conditions. The better photocatalytic performance shown by NAA-GIFs produced with T_P = 850 s is likely attributable to the enhanced mass transfer and light utilization efficiency by the photoactive TiO_2 layers at those spectral regions of higher irradiance due to the increment in T_P that results in longer L_{TP}.

Figure 4b shows the fitting lines for the photocatalytic degradation of RhoB by TiO_2-modified NAA-GIFs produced with T_P = 550, 650, 750 and 850 s, the k values of which were found to be 0.39 ± 0.02, 0.27 ± 0.01, 0.30 ± 0.01 and 0.31 ± 0.01 h^{-1}, respectively (**Table 1**). The best photocatalytic performance was achieved by TiO_2-modified NAA-GIFs produced with T_P = 550 s, which is ~21 to 31% higher than that shown by NAA-GIFs produced with longer anodization periods (i.e. 650, 750 and 850 s). As **Figure 4e** shows, the red edge of the PSB of TiO_2-functionalized NAA-GIFs fabricated with T_P = 550 s is positioned within the absorption band of RhoB, while the blue edge falls outside of the absorption region (i.e. $\lambda_{Blue\text{-}}$

$_{550s}$ = 466 nm, $\lambda_{Red\text{-}550s}$ = 527 nm and $\lambda_{Abs\text{-}RhoB}$ = 554 nm). Similarly, the blue edge of the PSB of NAA-GIFs fabricated with T_P = 750 s is partially within the absorption range of RhoB (i.e. $\lambda_{Blue\text{-}650s}$ = 543 nm). The red edge of the PSB of NAA-GIFs are produced with T_P = 550 s is within the absorption band of RhoB, leading to an enhanced absorption of light that results in the highest degradation rate for RhoB ($k_{RhoB\text{-}550s}$ = 0.39 ± 0.02 h^{-1}) due to the generation of extra e^-/h^+ pairs at these spectral regions. This phenomenon is confirmed in the case of the blue edge of the PSB of NAA-GIFs fabricated with T_P = 750 s, although the photocatalytic performance of this configuration is less photocatalytically efficient ($k_{RhoB\text{-}750s}$ = 0.30 ± 0.01 h^{-1}). The PSB of TiO_2-modified NAA-GIFs produced with T_P = 650 s is approximately at the center of the absorption band of RhoB. However, these PCs achieved the worst photocatalytic degradation performance for RhoB molecules ($k_{RhoB\text{-}650s}$ = 0.27 ± 0.01 h^{-1}). As **Figure S5** reveals, the intensity of the absorption band of RhoB (i.e. ~3.6 a.u.) is significantly higher than that of MO (i.e. ~1.5 a.u.) at its central position ($\lambda_{Abs\text{-}RhoB}$ = 554 nm). At these spectral regions, RhoB molecules absorb most of the incoming light that propagates through the aqueous organic dye before it reaches the surface of the TiO_2-NAA-GIFs, reducing the photocatalytic performance of the material due to light screening effect. The PSB of TiO_2-modified NAA-GIFs produced with T_P = 850 s is completely outside the absorption band of RhoB (**Figure 4e**), although the photocatalytic performance shown by these photoactive PCs to degrade RhoB was found to be comparable to that achieved by NAA-GIFs fabricated with T_P = 750 s ($k_{RhoB\text{-}850s}$ = 0.31 ± 0.01 h^{-1}). In this scenario, photocatalytic performance is exclusively dependent on the geometric features of the PC and on the irradiation conditions than on the 'slow photon' effect. These NAA-GIFs have the longest period length (L_{TP}), which facilitates the mass transfer of reactive species along the nanoporous structure and increases the number of photoactive sites, leading to enhanced photodegradation rates. Our analysis clearly demonstrates that the most effective approach to utilize 'slow photon' effect

in TiO_2-modified NAA-GIFs to degrade RhoB molecules is to match the red edge of the PSB of these PCs with the blue and red edges of the absorption band of RhoB.

Figure 4c presents the photocatalytic degradation of MB by TiO_2-functionalized NAA-GIFs produced with T_P = 550, 650, 750 and 850 s. The degradation rates achieved by these photoactive PCs were found to be k = 1.07 ± 0.04, 1.84 ± 0.09, 0.36 ± 0.01 and 2.10 ± 0.07 h^{-1}, respectively (**Table 1**). The highest photodegradation rate of MB was performed by TiO_2-modified NAA-GIF fabricated with T_P = 850 s, which was from ~11 to 83% better than NAA-GIF counterparts produced with shorter anodization periods. As **Figure 4f** shows, the red edge of the PSB of these PCs matches the red edge of the absorption band of MB (i.e. $\lambda_{Blue\text{-}850s}$ = 685 nm, $\lambda_{Red\text{-}850s}$ = 750 nm and $\lambda_{Abs\text{-}MB}$ = 664 nm). On the other hand, TiO_2-modified NAA-GIFs produced with T_P = 750 s displayed the worst performing photocatalytic performance to degrade MB (i.e. $k_{MB\text{-}750s}$ = 0.36 ± 0.01 h^{-1}), which was approximately six times slower rate than that of NAA-GIFs produced with T_P = 850 s). According to **Figure 4f**, the PSB of TiO_2-modified NAA-GIFs fabricated with T_P = 750 s is entirely within the absorption band of MB (i.e. $\lambda_{Blue\text{-}750s}$ = 621 nm, $\lambda_{Red\text{-}750s}$ = 702 nm and $\lambda_{Abs\text{-}MB}$ = 664 nm). Likewise in the photocatalytic degradation of RhoB, the poor photocatalytic performance shown by these PCs can be ascribed to the high absorbance intensity of MB (i.e. ~2.9 a.u.) (**Figure S5 – Supporting Information**), which hinder the incoming photons from reaching the surface of TiO_2-modified NAA-GIFs to generate e^-/h^+ pairs to photodegrade MB molecules absorbed onto the inner surfaces. As **Figure 4c** shows, TiO_2-functionalized NAA-GIFs produced with T_P = 650 s achieved the second-best performance to degrade MB molecules, with $k_{MB\text{-}650s}$ = 1.84 ± 0.09 h^{-1}. An analysis of the relative position of the blue and red edges of the PSB of these photoactive PC structures with respect to the absorption band of MB (**Figure 4f**) reveals that the PSB's blue edge is well-matched with the blue edge of the absorption band of MB (i.e. $\lambda_{Blue\text{-}650s}$ = 531 nm, $\lambda_{Red\text{-}650s}$ = 602 nm and $\lambda_{Abs\text{-}MB}$ = 664 nm).

This configuration results in enhancement of the photodegradation of these molecules due to 'slow photon' effect. However, these TiO_2-modified NAA-GIFs undergo photodegradation at a rate ~11% slower than those produced at T_P = 850 s. Finally, **Figure 4c** shows that the PSB of TiO_2-functionalized NAA-GIFs produced with T_P = 550 s is located completely away from the absorption band of MB. Therefore, the photocatalytic performance to degrade the MB molecules by these PCs is associated with the geometric features of the NAA-GIF structure and the irradiation conditions, without contribution from 'slow photon' effects. These PC structures showed the second-worst degradation rate of this set of NAA-GIFs, with a $k_{MB\text{-}550s}$ = 1.07 ± 0.04 h^{-1}.

To summarize, a systematic analysis on the effect of T_P on the photocatalytic degradation of three model organic dye molecules (MO, RhoB and MB) by TiO_2-functionalized NAA-GIFs is presented. Our study establishes that the maximum degradation rates for MO, RhoB and MB were $k_{MO\text{-}650s}$ = 0.25 ± 0.01 h^{-1}, $k_{RhoB\text{-}550s}$ = 0.39 ± 0.02 h^{-1} and $k_{MB\text{-}850s}$ = 2.10 ± 0.07 h^{-1}, which is achieved by TiO_2-functionalized NAA-GIFs produced with T_P = 650, 550 and 850 s, respectively. Our results demonstrate that a rational design of the PSB these PCs with respect to the absorption band of these dyes can lead to a significant enhancement of the photodegradation rate. Optimal design of these composite photocatalysts requires careful consideration of the position of the blue and red edges of the PSB with respect to the absorption band of the dye molecule to be degraded. However, the pairing between maximum of the absorption band of the dye molecules and the PSB worsens significantly the overall photocatalytic performance due to light screening effect. When the characteristic PSB falls completely outside of the absorption band of the organic dyes, the photocatalytic performance of TiO_2-modified NAA-GIFs is solely associated with the geometric features of the nanoporous matrix and it enhances with increasing T_P due to enhanced mass transfer, increasing number of photoactive sites and light irradiation utilization. The nature of the dye

molecules and their interaction with the photocatalyst surface is also a critical contributing factor for the correct interpretation of the obtained photodegradation rates.

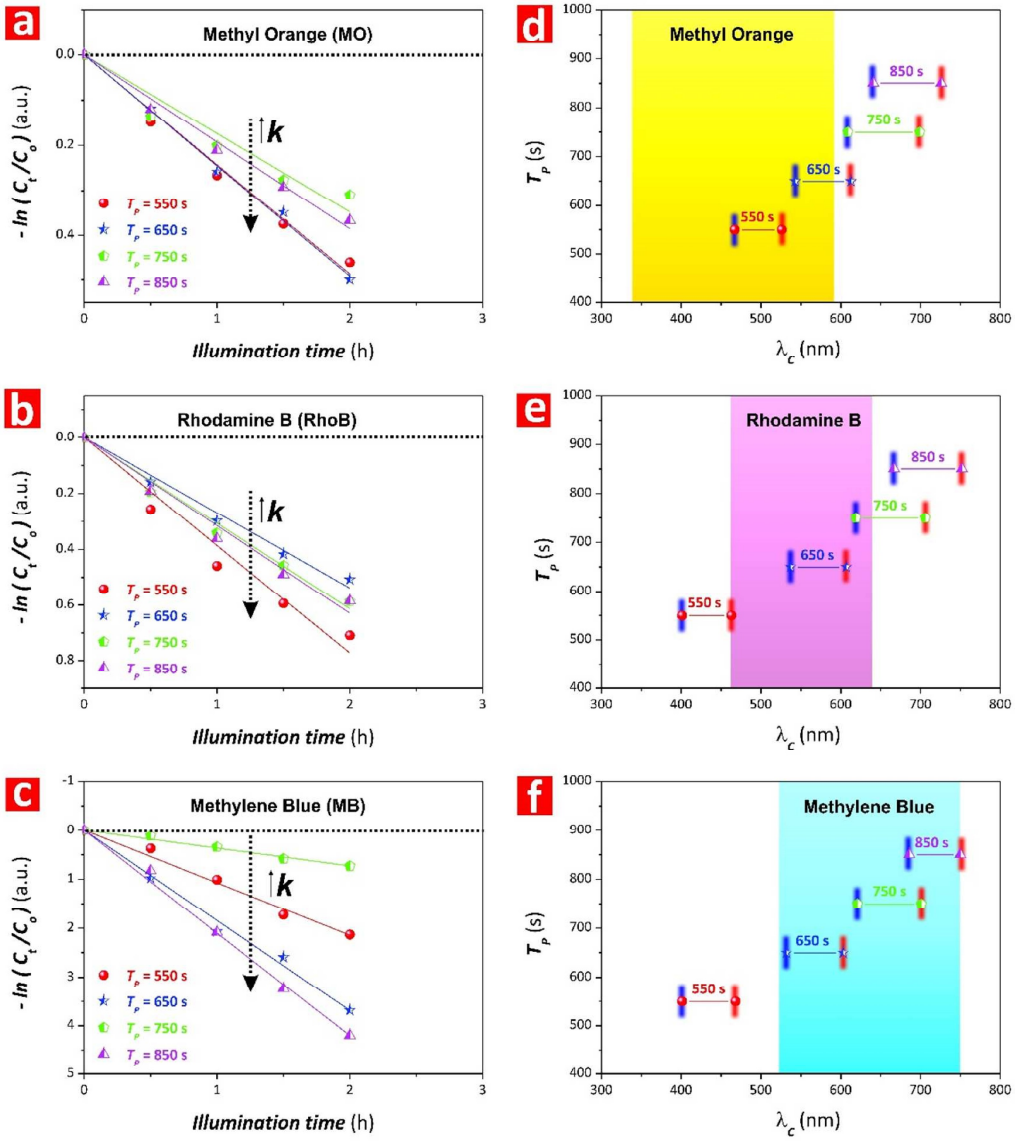

Figure 4. Tuning the blue and red edges of the PSB of TiO_2-functionalized NAA-GIFs produced with different T_P to utilize the 'slow photon' effect for the photocatalytic degradation of model organic dyes. a-c) Photocatalytic degradation kinetics of MO, RhoB and MB by TiO_2-modified NAA-GIFs fabricated with different T_P = 550, 650, 750 and 850 s under controlled irradiation conditions, respectively (note: black dotted lines denote the photodegradation of the corresponding dye in control NAA-GIFs without functional TiO_2 layer). d-f) Relative position of the blue and red edges of the characteristic PSB of TiO_2-functionalized NAA-GIFs produced with T_P = 550, 650, 750 and 850 s and the absorption band of MO, RhoB and MB, respectively (note: blue and red vertical lines on the PSB of NAA-GIFs correspond to the position of the blue and red edges of the PSB).

For instance, our study established that the average degradation rates for RhoB and MB (i.e. 0.32 ± 0.02 and 1.34 ± 0.04 h^{-1}) and were faster than that of MO (i.e. 0.21 ± 0.04 h^{-1}). RhoB and MB are positively charged molecules, whereas the surface of the photoactive TiO_2 layer is negatively charged at the pH conditions in which our study was performed (pH = 5.5).[37]

This results in a strong electrostatic attraction between the organic dye molecules and the functional TiO_2 layer. The higher number of adsorbed molecules onto the photoactive surface leads to an enhancement of the overall photodegradation rate. In contrast, MO is an anionic organic dye with negative charge that is electrostatically repulsed by the negatively charged surface of TiO_2. This reduces the amount of MO molecules absorbed onto the photo-functional surface, worsening the overall photocatalytic degradation performance of the system.[38]

3.5.2. Effect of Anodization Time on the Photocatalytic Performance of TiO_2-NAA-GIFs

The effect of the anodization time (or number of anodization pulses in SPA) on the photocatalytic performance associated with the degradation of two model dyes (i.e. RhoB and MB) was also studied to further define the capabilities of TiO_2-functionalized NAA-GIFs as photocatalyst platforms. A set of NAA-GIFs was fabricated by systematically modifying the anodization time (t_{An}) from 5 to 20 h (or from 22 to 85 pulses) with Δt_{An} = 5 h (or ΔN_P = 22 pulses), while other anodization parameters were kept constant (i.e. T_P = 850 s, A_J = 0.420 mA cm^{-2}, J_{Offset} = 0.280 mA cm^{-2} and t_{pw} = 6 min). The surface of these NAA-GIFs was functionalized with photoactive layers of TiO_2 following the above-mentioned sol-gel protocol. **Figure 5** and **Table 2** summarize the photocatalytic degradation performance of TiO_2-modified NAA-GIFs produced with t_{An} = 5, 10, 15 and 20 h for RhoB and MB with linearized pseudo-first order kinetics, where the insets represent the degradation rates (k) (i.e. slopes of fitting lines) for each system. **Figure 5a** displays photocatalytic performance of

TiO_2-functionalized NAA-GIFs as a function of t_{An} for RhoB. Our results reveal that these photoactive PCs degrade RhoB molecules at a rate of 0.28 ± 0.02, 0.27 ± 0.02, 0.22 ± 0.02 and 0.31 ± 0.02 h^{-1} for t_{An} = 5, 10, 15 and 20 h, respectively. In general, the photocatalytic performance shown by these TiO_2-funtionalized NAA-GIFs is comparable, with an average degradation rate of 0.27 ± 0.02 h^{-1}. However, it is apparent that the most optimal platforms are those fabricated with t_{An} = 20 h (i.e. 85 pulses), which provided the best performance as compared to their counterparts produced with shorter anodization time (i.e. 10 to 29% enhancement). The total thickness of NAA-GIFs is directly proportional to the anodization time (i.e. number of anodization pulses).[39] This thickness increment leads to an enhancement of the total light absorption by the composite PC structure,[40] enabling the generation of extra e^-/h^+ pairs that can be employed to increase the photodegradation rate of RhoB molecules. The performance of TiO_2-functionalized NAA-GIFs for the photocatalytic degradation of MB is shown in **Figure 5b**. These results confirm the same trend in the photodegradation rates as a function of the anodization time than that observed for RhoB molecules, where the *k* values were found to be 1.41 ± 0.04, 1.32 ± 0.02, 1.26 ± 0.03 and 2.10 ± 0.07 h^{-1} for TiO_2-functionalized NAA-GIFs produced with t_{An} = 5, 10, 15 and 20 h, respectively. The rates of photodegradation for TiO_2-NAA-GIFs produced with t_{An} = 5, 10 and 15 h are comparable. However, the fastest degradation rate was achieved by those photoactive PCs produced with t_{An} = 20 h (i.e. 85 pulses), which provided ~33 to 46% enhancement as compared to their counterparts produced with shorter anodization time.

This analysis demonstrates that TiO_2-modified NAA-GIFs produced with t_{An} = 20 h are the optimal composite PC platforms for the photocatalytic degradation of RhoB and MB dyes. However, the photodegradation of MB molecules was found to be more dependent on t_{An} than RhoB, as demonstrated by the enhancement in degradation rates (i.e. up to 29 and 46% for RhoB and MB, respectively). Our study also reveals that the average *k* value for the

photodegradation of MB is larger than that of RhoB by ~6 times (i.e. 1.52 ± 0.39 and 0.27 ± 0.04 h^{-1}, respectively), where this difference is in good agreement with the results obtained for the photocatalytic degradation of these organic dyes by TiO_2-modified NAA-GIFs produced with different T_P.

Table 2. Values of the kinetic constant (k) for the photodegradation of RhoB and MB molecules in TiO_2-functionalized NAA-GIFs produced with t_{An} = 5, 10, 15 and 20 h.

	Anodization Time			
Organic Dye	5 h	10 h	15 h	20 h
RhoB	0.28 ± 0.02 h^{-1}	0.27 ± 0.02 h^{-1}	0.22 ± 0.02 h^{-1}	0.31 ± 0.01 h^{-1}
MB	1.41 ± 0.04 h^{-1}	1.32 ± 0.02 h^{-1}	1.26 ± 0.03 h^{-1}	2.10 ± 0.07 h^{-1}

3.6. Photocatalytic Degradation Mechanism. A possible photocatalytic degradation mechanism using TiO_2-modified NAA-GIFs with the aid of H_2O_2 under visible-NIR light irradiation ($400 < \lambda < 1000$ nm) is proposed based on the above results. Under light irradiation, e^-/h^+ pairs in the photoactive TiO_2 layer deposited onto the inner surface of NAA-GIFs are generated in the conduction and valence bands, respectively. Oxidation of H_2O induced by photogenerated holes forms $^{\cdot}OH$ radicals that degrade the model organic dye molecules, decomposing these organic compounds into CO_2 and H_2O. H_2O_2 is added as a primary electron acceptor to form $^{\cdot}OH$ radicals and OH^- ions, which are oxidized by the photogenerated holes to $^{\cdot}OH$ radicals. The enhanced photodegradation rates observed in our study can be associated with the 'slow photon' effect, which further facilitates the lifetime and photogeneration of charge carriers, and with the mass transfer and photoactive sites in the nanoporous photonic structure of NAA-GIFs.

Photons from high irradiance regions (i.e. visible and NIR) are collected by the underlying NAA-based PC structure and utilized by the photoactive TiO_2 functional layer to generate e^-/h^+ pairs. Photocatalytic enhancement is due to the presence of photons with reduced group velocity localized at frequencies of high irradiance that match with the edges of the characteristic PSB of NAA-GIFs. This enhancement was found to be maximum when the blue and red edges of the PSB are located at the proximity of the blue and red sides of the absorbance band of the model dye molecules. However, the high absorption of light of organic dyes at the center of their absorbance band minimizes the amount of light that reaches the photoactive layer of TiO_2-functionalized NAA-GIFs, reducing significantly the overall photodegradation rate. This effect is particularly significant for organic dyes with high absorption bands, such as RhoB and MB. Therefore, the absorption intensity and position of the absorbance band of organic dyes and the relative positioning of the edges of the PSB are critical factors to consider in order to make an optimal utilization of the 'slow photon' effect for enhanced photocatalytic applications by a rational management of photons at the nanoscale.

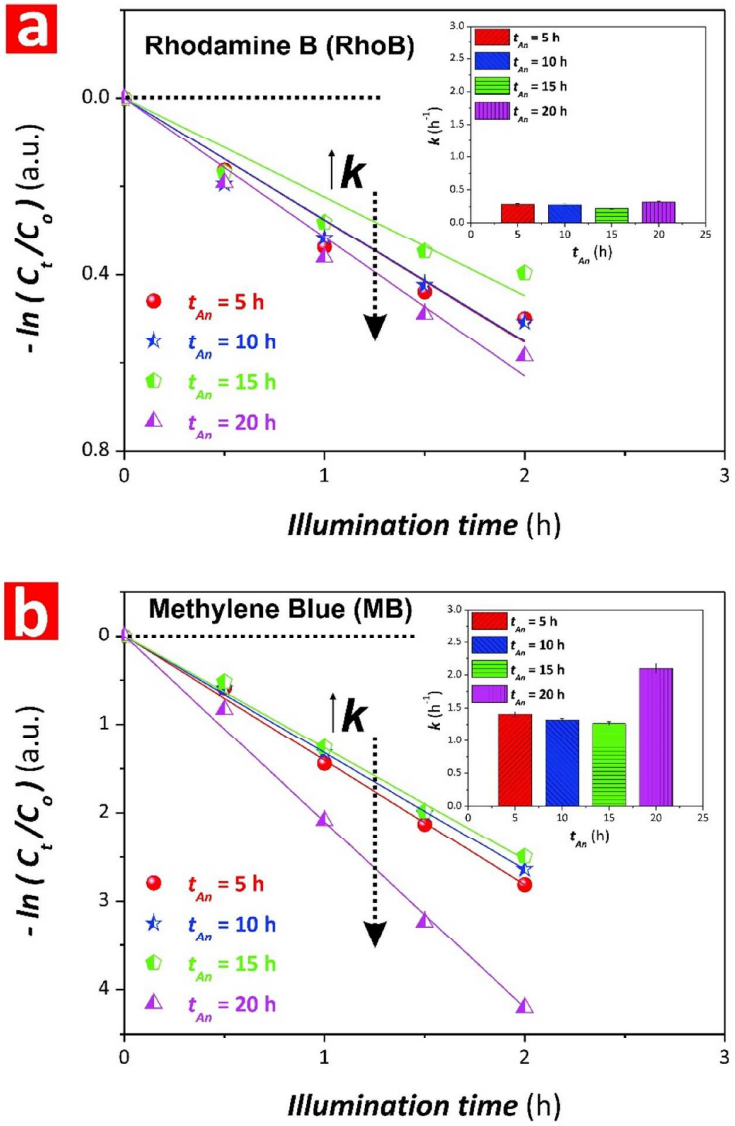

Figure 5. Effect of the anodization time (t_{An}) of TiO_2-functionalized NAA-GIFs on the photocatalytic degradation of model organic dyes. a and b) Photocatalytic degradation kinetics of RhoB and MB in TiO_2-modified NAA-GIFs produced with t_{An} = 5, 10, 15 and 20 h under controlled light irradiation, respectively (insets compile the values of the kinetic constant (k) for the photocatalytic degradation of these model organic dyes) (note: black dotted lines denote the photodegradation of the corresponding dye in control NAA-GIFs without functional TiO_2 layer).

To date, some proof-of-concept studies have identified and utilized the 'slow photon' effect in different photonic crystal structures (**Table 3**). For instance, Zheng *et al.* developed 3D TiO_2 inverted opal PCs featuring different pore sizes (i.e. from 270 to 460 nm) and assessed the photodegradation of RhoB, MO and MB under controlled illumination conditions.[38] The

performance of the system to degrade these dyes was assessed under visible light irradiation conditions. The photocatalytic performance of 3D TiO_2 inverted opal PCs was found to be k_{RhoB} = 0.47 h^{-1}, k_{MO} = 0.01h^{-1} and k_{MB} = 1.32 h^{-1}, respectively. Although the degradation rate for RhoB molecules was slightly higher than that achieved by our system (i.e. ~17% enhancement), TiO_2-functionalized NAA-GIFs showed a much superior performance to photodegrade MO and MB molecules (i.e. ~96% and ~37% enhancement, respectively).

Fabrication of nanotubular TiO_2 structures by direct anodization of titanium substrates enables the development of TiO_2-based photocatalyst PCs. However, the controllability and versatility of this method to engineer the effective medium of these PCs is limited. To date, several studies have explored the potential applicability of this material for photocatalysis. 1D nanotubular TiO_2 PCs provided degradations rates of k_{RhoB} = 0.195 h^{-1}, k_{MO} = 0.045 h^{-1} and k_{MB} = 2.00 h^{-1} under visible light irradiation.[41-43] Under the conditions used in our study (visible-NIR irradiation), TiO_2-modified NAA-GIFs outperform significantly 1D nanotubular TiO_2 PCs, with a performance enhancement of ~50%, ~82% and ~21% to degrade RhoB, MO and MB molecules, respectively.

Semiconductor nanoparticles are the benchmark and most widely investigated photocatalysts platforms in photocatalysis. Several studies have reported photodegradation of RhoB, MO and MB using P25 TiO_2 nanoparticles under controlled visible illumination conditions. The best performances achieved by this system were k_{RhoB} = 0.47 h^{-1}, k_{MO} = 0.24 h^{-1} and k_{MB} = 1.5 h^{-1}.[38,43,44] Photodegradation performance of P25 TiO_2 nanoparticles for RhoB was ~17% superior than that of TiO_2-functionalized NAA-GIFs. However, our system outperformed this photocatalyst benchmark material in the degradation of MO and MB, with an enhancement of ~4% and ~29%, respectively.

These results demonstrate the potential of TiO_2-modified NAA-GIFs as a photocatalyst platform, where optoelectronic properties can be precisely engineered to achieve unprecedented performances in photocatalysis applications.

Table 3. Compilation of representative values of the kinetic constant (k) for the photodegradation of MO, RhoB and MB molecules in different TiO_2-based photocatalyst systems.

TiO_2-Based Material	**Organic Dye**	***k*** **(h^{-1})**	**Reference**
3D Inverted Opal PCs	MO	0.01	38
	RhoB	0.47	38
	MB	1.32	38
Anodic Nanotubular PCs	MO	0.045	42
	RhoB	0.195	41
	MB	2.00	43
P25 Nanoparticles	MO	0.24	44
	RhoB	0.47	38
	MB	1.50	43
NAA-GIFs	MO	0.25	This Study
	RhoB	0.39	This Study
	MB	2.10	This Study

CONCLUSIONS

To summarize, we have performed first study assessing the capability of photoactive NAA-based PC structures functionalized with TiO_2 layers to enhance the performance of photocatalytic reactions by 'slow photon' effect. Manipulation of various anodization parameters (i.e. pore widening time, anodization period and anodization time) during the fabrication of these PC structures enables precise engineering of features (i.e. position and bandwidth) of their PSB across the spectral regions. The photon-to-electron conversion rate in TiO_2-modified NAA-GIFs was found to be dependent on the position of edges of the characteristic PSB as well as on the absorption range, absorbance intensity and properties of model organic dyes under simulated solar light irradiation. A careful design of the position of the edges of the PSB of photoactive NAA-GIFs with respect to the absorption band of organic dyes was found to enhance the photodegradation rate of these molecules significantly by 'slow photon' effect. This approach enables the utilization of photons from high irradiance regions (i.e. visible and NIR) to generate extra e^-/h^+ pairs, overcoming the intrinsic limitation of the photoactive material (i.e. TiO_2 – constricted to the UV range). Our study reveals that TiO_2-functionalized NAA-GIFs produced with T_P values of 550, 650 and 850 s show the best photocatalytic performances to degrade rhodamine B, methyl orange and methylene blue, respectively (i.e. $k_{RhoB\text{-}550s}$ = 0.39 ± 0.02 h^{-1}, $k_{MO\text{-}650s}$ = 0.25 ± 0.01 h^{-1} and $k_{MB\text{-}850s}$ = 2.10 ± 0.07 h^{-1}, respectively). In many cases, our system outperformed other photocatalyst platforms in the photodegradation of these model molecules, demonstrating a promising potential in photocatalysis applications.

Pairing between the absorption band of the organic dye with the edges of the PSB of photoactive NAA-GIFs was found to be optimal to enhance the photodegradation of methyl orange molecules due to the low absorption intensity. However, in the case of highly absorbing dye molecules (i.e. rhodamine B and methylene blue), optimal utilization of the

'slow photon' effect requires alignment of the blue or red edges of the PSB with the edges of the absorption band of the dye to avoid light screening effects. When the characteristic PSB of photoactive NAA-GIFs falls completely outside of the absorption band of the organic dyes, the photocatalytic performance is solely associated with the geometric features of the PC structure. In such scenario, NAA-GIFs produced with longer anodization period achieve better degradation rages due to the longer period length within the NAA-GIF structure, which enhances the mass transfer of reactive species and increases the number of photoactive sites. Our study also reveals that the optimal anodization time (i.e. number of anodization pulses) for the efficient photocatalytic degradation of organic dyes is 20 h (i.e. 85 pulses at T_P = 850 s), independently on the type of organic dye to be degraded. The properties of the model organic dye (i.e. charge and photosensitivity) play a critical role to dictate the overall photocatalytic performance of TiO_2-functionalized NAA-GIFs, where positively charged and more photosensitive molecules (i.e. RhoB and MB) degrade at faster rates.

Our comprehensive study demonstrates that the development of photoactive NAA-GIFs with rationally engineered optical and photocatalytic properties can enhance photon-to-electron conversion rates significantly, providing new opportunities for the development of environmental friendly, economical and high-performance photocatalysts with broad applicability in environmental remediation and clean energy generation.

AUTHOR INFORMATION

Corresponding Authors

Doctor Abel Santos
Research for Impact Fellow – Lecturer
School of Chemical Engineering – The University of Adelaide
Phone: +61 8 8313 1535
Email: abel.santos@adelaide.edu.au
Web page: http://www.adelaide.edu.au/directory/abel.santos

Professor Andrew Abell
Professor of Chemistry and node director of the ARC Centre of Excellence for Nanoscale Biophotonics
School of Chemistry and Physics – The University of Adelaide
Phone: + 61 8 8313 5652
Email: Andrew.abell@adelaide.edu.au
Web page: http://researchers.adelaide.edu.au/profile/andrew.abell#contact-details

Notes

The authors declare no competing financial interest.

ACKNOWLEDGEMENT

Authors thank the support provided by the Australian Research Council (ARC) through the grants number DE140100549 and CE140100003, the School of Chemical Engineering, the University of Adelaide (UoA), the Institute for Photonics and Advanced Sensing (IPAS), and the ARC Centre of Excellence for Nanoscale BioPhotonics (CNBP). Authors thank the Adelaide Microscopy (AM) centre for FEG-SEM and EDX characterization.

ASSOCIATED CONTENT

Supporting Information. The Supporting Information file provides further information on the calibration lines correlating dye concentration and absorbance, transmission spectra and digital pictures of NAA-GIFs, chemical analysis confirming the deposition of TiO_2 on the surface of NAA-GIFs through EDX, FTIR and XRD spectra, the PSB of NAA-GIFs at different TiO_2 deposition time, the absorption spectra of methyl orange, methylene blue and rhodamine B as well as the spectrum for the simulated solar light irradiation used to assess the photocatalytic performance of TiO_2-functionalized NAA-GIFs. This file also contains information about the residual concentration of each dye after 2 h of photocatalytic reaction in TiO_2-functionalized NAA-GIFs. This material is available free of charge via the Internet at http://pubs.acs.org.

REFERENCES

1. Fox, M. A.; Dulay, M. T. Heterogeneous Photocatalysis. *Chem. Rev.* **1993**, *93*, 341-357.

2. Liu, M.; Chen, Y.; Su, J.; Shi, J.; Wang, X.; Guo, L. Photocatalytic Hydrogen Production Using Twinned Nanocrystals and an Unanchored NiSx Co-Catalyst. *Nat. Energy* **2016**, *1*, 16151.

3. Mushtaq, F.; Asani, A.; Hoop, M.; Chen, X. -Z.; Ahmed, D.; Nelson, B. J.; Pané, S. Highly Efficient Coaxial TiO_2□PtPd Tubular Nanomachines for Photocatalytic Water Purification with Multiple Locomotion Strategies. *Adv. Funct. Mater.* **2016**, *26*, 6995-7002.

4. Ren, H.; Koshy, P.; Chen, W. -F.; Qi, S.; Sorrell, C. C. Photocatalytic Materials and Technologies for Air Purification. *J. Hazard. Mater.* **2017**, *325*, 340-366.

5. Hirakawa, H.; Hashimoto, M.; Shiraishi, Y; Hirai, T. Photocatalytic Conversion of Nitrogen to Ammonia with Water on Surface Oxygen Vacancies of Titanium Dioxide. *J. Am. Chem. Soc.* **2017**, *139*, 10929-10936.

6. Tu, W.; Zhou, Y.; Zou, Z. Photocatalytic Conversion of CO_2 into Renewable Hydrocarbon Fuels: State-of-the-Art Accomplishment, Challenges, and Prospects. *Adv. Mater.* **2014**, *26*, 4607-4626.

7. Liu, J.; Zhao, H.; Wu, M.; Van der Schueren, B.; Li, Y.; Deparis, O.; Ye, J.; Ozin, G. A.; Hasan, T.; Su, B. -L. Slow Photons for Photocatalysis and Photovoltaics. *Adv. Mater.* **2017**, *29*, 1605349.

8. Baba, T. Slow Light in Photonic Crystals. *Nat. Photonics* **2008**, *2*, 465-473.

9. Noda, S.; Chutinan, A.; Imada, M. Trapping and Emission of Photons by a Single Defect in a Photonic Bandgap Structure. *Nature* **2000**, *407*, 608-610.

10. Noda, S.; Tomoda, K.; Yamamoto, N.; Chutinan, A. Full Three-Dimensional Photonic Bandgap Crystals at Near-Infrared Wavelengths. *Science* **2000**, *289*, 604-606.

11. Akahane, Y.; Asano, T.; Song, B.-S.; Noda, S. High Q-Photonic Nanocavity in a Two-Dimensional Photonic Crystal. *Nature* **2003**, *425*, 944-947.

12. Curti, M.; Schneider, J.; Bahnemann, D. W.; Mendive, C. B. Inverse Opal Photonic Crystals as a Strategy to Improve Photocatalysis: Underexplored Questions. *J. Phys. Chem. Lett.* **2015**, *6*, 3903-3910.

13. Wang, C.; Chen, D.; Ping, G. X.; Liu, S.; Huang, X. N.; Huang, Y. X.; Shu, K. Y.; Li, J. H. Controllable Synthesis of Well-Ordered TiO_2 Nanotubes in a Mixed Organic Electrolyte for High-Efficiency Photocatalysis. *Sci. China Chem.* **2012**, *55*, 2373-2380.

14. Qin, L.; Chen, Q.; Lan, R.; Jiang, R.; Quan, X.; Xu, B.; Zhang, F.; Jia, Y. Effect of Anodization Parameters on Morphology and Photocatalysis Properties of TiO_2 Nanotube Arrays. *J. Mater. Sci. Technol.* **2015**, *31*, 1059-1064.

15. Lee, K.; Mazare, A.; Schmuki, P. One-Dimensional Titanium Dioxide Nanomaterials: Nanotubes. *Chem. Rev.* **2014**, *114*, 9385-9454.

16. Santos, A.; Yoo, J. H.; Rohatgi, C. V.; Kumeria, T.; Wang, Y.; Losic, D. Realisation an Advanced Engineering of True Optical Rugate Filters Based on Nanoporous Anodic Alumina by Sinusoidal Pulse Anodisation. *Nanoscale* **2016**, *8*, 1360-1373.

17. Kumeria, T.; Santos, A.; Rahman, M. M.; Ferré-Borrull, J.; Marsal, L. F.; Losic, D. Advanced Structural Engineering of Nanoporous Photonic Structures: Tailoring Nanopore Architecture to Enhanced Sensing Properties. *ACS Photonics* **2014**, *1*, 1298-1306.

18. Santos, A. Nanoporous Anodic Alumina Photonic Crystals: Fundamentals, Developments and Perspectives. *J. Mater. Chem. C* **2017**, *5*, 5581-5599.

19. Santos, A.; Kumeria, T.; Losic, D. Nanoporous Anodic Alumina: A Versatile Platform for Optical Biosensors. *Materials* **2014**, *7*, 4297-4320.

20. Law, C. S.; Santos, A.; Nemati, M.; Losic, D. Structural Engineering of Nanoporous Anodic Alumina Photonic Crystals by Sawtooth-like Pulse Anodization. *ACS Appl. Mater. Interfaces* **2016**, *8*, 13542-13554.

21. Law, C. S.; Sylvia, G. M.; Nemati, M.; Yu, J.; Losic, D.; Abell, A. D.; Santos, A. Engineering of Surface Chemistry for Enhanced Sensitivity in Nanoporous Interferometric Sensing Platforms. *ACS Appl. Mater. Interfaces* **2017**, *9*, 8929-8940.

22. Wang, Y.; Chen, Y.; Kumeria, T.; Ding, F.; Evdokiou, A.; Losic, D.; Santos, A. Facile Synthesis of Optical Microcavities by a Rationally Designed Anodization Approach: Tailoring Photonic Signals by Nanopore Structure. *ACS Appl. Mater. Interfaces* **2015**, *7*, 9879-9888.

23. Chen, Y.; Santos, A.; Ho, D.; Wang, Y.; Kumeria, T.; Li, J.; Wang, C.; Losic, D. On the Generation of Interferometric Colors in High Purity and Technical Grade Aluminum: An

Alternative Green Process for Metal Finishing Industry. *Electrochim. Acta* **2015**, 174, 672-681.

24. Lee, C.-Y.; Schmuki, P. Engineering of Self-Organizing Electrochemistry: Porous Alumina and Titania Nanotubes. In *Electrochemical Engineering Across Scales: From Molecules to Proceses*; Alkire, R. C., Bartlett, P. N., Lipkowski, J., Eds.; John Wiley & Sons: Weinheim, 2015; Vol. 15, pp 145-192.

25. Wu, J.; Liu, B.; Ren, Z.; Ni, M.; Li, C.; Gong, Y.; Qin, W., Huang, Y.; Sun, C. Q.; Liu, X. CuS/RGO Hybrid Photocatalyst for Full Solar Spectrum Photoreduction from UV/Vis to Near-Infrared Light. *J. Colloid Interface Sci.* **2018**, *517*, 80-85.

26. Wang, Y.; Santos, A.; Evdokiou, A.; Losic, D. Rational Design of Ultra-Short Anodic Alumina Nanotubes by Short-Time Pulse Anodizaion. *Electrochim. Acta* **2015**, *154*, 379-386.

27. Santos, A.; Formentin, P.; Ferré-Borrull, J.; Pallarès, J.; Marsal, L. F. Nanoporous Anodic Alumina Obtained Without Protective Oxide Layer by Hard Anodization. *Mater. Lett.* **2012**, *67*, 296-299.

28. Massard, C.; Pairis, S.; Raspal, V.; Sibaud, Y.; Awitor, K. Fabrication of TiO_2 Nanotanks Embedded in a Nanoporous Alumina Template. *J. Nanomater.* **2015**, *2015*, 452148.

29. Abràmoff, M. D.; Magalhães, P. J.; Ram, S. J. Image Processing with ImageJ. *Biophotonics Inter.* **2004**, *11*, 36-42.

30. León, A.; Reuquen, P.; Garín, C.; Segura, R.; Vargas, P.; Zapata, P.; Orihuela, P. A. FTIR and Raman Characterization of TiO_2 Nanoparticles Coated with Polyethylene Glycol as Carrier for 2-Methoxyestradiol. *Appl. Sci.* **2017**, *7*, 49.

31. Chellappa, M.; Anjaneyulu, U.; Manivasagam, G.; Vijayalakshmi, U. Preparation and Evaluation of the Cytotoxic Nature of TiO_2 Nanoparticles by Direct Contact Method. *Int. J. Nanomedicine* **2015**, *10*, 31-41.

32. Kumeria, T.; Rahman, M. M.; Santos, A.; Ferré-Borrull, J.; Marsal, L. F.; Losic, D. Structural and Optical Nanoengineering of Nanoporous Anodic Alumina Rugate Filters for Real-Time and Label-Free Biosensing Applications. *Anal. Chem.* **2014**, *86*, 1837-1844.

33. Zhang, Z.; Wu, H. Multiple Band Light Trapping in Ultraviolet, Visible and Near Infrared Regions with TiO_2 Based Photonic Materials. *Chem. Commun.* **2014**, *50*, 14179-14182.

34. Nishimura, S.; Abrams, N.; Lewis, B. A.; Halaoui, L. I.; Malluok, T. E.; Benkstein, K.D.; van de Lagemaat, J.; Frank, A. J. Standing Wave Enhancement of Red Absorbance and Photocurrent in Dye-Sensitized Titanium Dioxide Photoelectrodes Coupled To Photonic Crystals. *J. Am. Chem. Soc.* **2003**, *125*, 6306-6310.

35. Deparis, O.; Mouchet, S. R.; Su, B.-L. Light Harvesting in Photonic Crystals Revisited: Why do Slow Photons at the Blue Edge Enhance Absorption? *Phys. Chem. Chem. Phys.* **2015**, *17*, 30525-30532.

36. Li, Y.; Kunitake, T.; Fujikawa, S. Efficient Fabrication and Enhanced Photocatalytic Activities of 3D-Ordered Films of Titania Hollow Spheres. *J. Phys. Chem. B* **2006**, *110*, 13000-13004.

37. *Design of Advanced Photocatalytic Materials for Energy and Environmental Applications*; Coronado, J. M., Fresno, F., Hernández-Alonso, M. D., Portela, R., Eds.; Springer: London, 2013.

38. Zheng, X.; Meng, S.; Chen, J.; Wang, J.; Xian, J.; Shao, Y.; Fu, X.; Li, D. Titanium Dioxide Photonic Crystals with Enhanced Photocatalytic Activity: Matching Photonic Band Gaps of TiO_2 to the Absorption Peaks of Dyes. *J. Phys. Chem. C* **2013**, *117*, 21263-21273.

39. Santos, A.; Balderrama, V. S.; Alba, M.; Formentín, P.; Ferré-Borrull, J.; Pallarès, J.; Marsal, L. F. Nanoporous Anodic Alumina Barcodes: Toward Smart Optical Biosensors. *Adv. Mater.* **2012**, *24*, 1050-1054.

40. Brzózka, A.; Brudzisz, A.; Hnida, K.; Sulka, G. D. Chemical and Structural Modifications of Nanoporous Alumina and Its Optical Properties. In *Electrochemically Engineered Nanoporous Materials: Methods, Properties and Applications*; Losic, D., Santos, A., Eds.; Springer International Publishing: Cham, 2015; Vol. 220, pp. 219-288.

41. Geng, Z.; Zhang, Y.; Yuan, X.; Huo, M.; Zhao, Y.; Lu, Y.; Qiu, Y. Incorporation of Cu_2O nanocrystals into TiO_2 Photonic Crystal for Enhanced UV-Visible Light Driven Photocatalysis. *J. Alloys Compd.* **2015**, *644*, 734-741.

42. Lu, Y.; Yu, H.; Chen, S.; Quan, X.; Zhao, H. Integrating Plasmonic Nanoparticles with TiO_2 Photonic Crystal for Enhancement of Visible-Light Driven Photocatalysis. *Environ. Sci. Technol.* **2012**, *46*, 1724-1730.

43. Sheng, X.; Liu, J.; Coronel, N.; Agarwal, A. M.; Michel, J.; Kimerling, L. C. Integration of Self-Assembled Porous Alumina and Distributed Bragg Reflector for Light Trapping in Si Photovoltaic Devices. *IEEE Photonics Technol. Lett.* **2010**, *22*, 1394-1396.

44. Guo, M.; Xie, K.; Wang, Y.; Zhou, L.; Huang, H. Aperiodic TiO_2 Nanotube Photonic Crystal: Full-Visible-Spectrum Solar Light Harvesting in Photovoltaic Devices. *Sci. Rep.* **2014**, *4*, 6442.

TABLE OF CONTENTS